Chinese Chemical Letters 34 (2023) 108239

Contents lists available at ScienceDirect

Chinese Chemical Letters

journal homepage: www.elsevier.com/locate/cclet

β-Cyclodextrin derived full-spectrum fluorescent carbon dots: The formation process investigation and biological applications

Peide Zhu[a,1], Wenjing Li[b,1], Yuqi Zhang[a,1], Qiang Sun[c], Yi Lin[b], Ailin Qiu[b], Xinyi Chen[a], Yujin Zhou[b], Guangfu Wu[a], Yifan Li[b], Zhiqiang Yu[d], Quan Xu[a,*], Dixian Luo[b,*], Lulu Cai[c,*]

[a] State Key Laboratory of Heavy Oil Processing, China University of Petroleum-Beijing, Beijing 102249, China
[b] Department of Laboratory Medicine, Huazhong University of Science and Technology Union Shenzhen Hospital (Nanshan Hospital), Shenzhen 518052, China
[c] Personalized Drug Therapy Key Laboratory of Sichuan Province, Department of Pharmacy, Sichuan Provincial People's Hospital, University of Electronic Science and Technology of China, Chengdu 611731, China
[d] Department of Laboratory Medicine, Dongguan Institute of Clinical Cancer Research, Affiliated Dongguan Hospital, Southern Medical University, Dongguan 523018, China

ARTICLE INFO

Article history:
Received 19 September 2022
Revised 10 February 2023
Accepted 15 February 2023
Available online 24 February 2023

Keywords:
Carbon dots
Multi-emission
Fluorescence mechanism
Mitochondrial targeting
Color tenability
Fluorescence imaging

ABSTRACT

Carbon dots (CDs), a new building unit, have been revolutionizing the fields of biomedicine, bioimaging, and optoelectronics with their excellent physical, chemical, and biological properties. However, the difficulty of preparing excitation-dependent full-spectrum fluorescent CDs has seriously hindered their further research in fluorescence emission mechanisms and biomedicine. Here, we report full-spectrum fluorescent CDs that exhibit controlled emission changes from purple (380 nm) to red (613 nm) at room temperature by changing the excitation wavelength, and the excitation dependence was closely related to the regulation of sp^2 and sp^3 hybrid carbon structures by β-cyclodextrin-related groups. In addition, by regulating the content of β-cyclodextrin, the optimal quantum yields of full-spectrum fluorescent CDs were 8.97%, 8.35%, 7.90%, 9.69% and 17.4% at the excitation wavelengths of 340, 350, 390, 410 and 540 nm, respectively. Due to their excellent biocompatibility and color tunability, full-spectrum fluorescent CDs emitted bright and steady purple, blue, green, yellow, and red fluorescence in MCF-7 cells. Moreover, we optimized the imaging conditions of CDs and mitochondrial-specific dyes; and realized the mitochondrial-targeted co-localization imaging of purple, blue and green fluorescence. After that, we also explored the effect of full-spectrum fluorescent CDs *in vivo* fluorescence imaging through the intratumorally, subcutaneously, and caudal vein, and found that full-spectrum fluorescent CDs had good fluorescence imaging ability *in vivo*.

Multi-color emission materials derived from tunable photoluminescence are of particular research interest owing to their latent utilization in microlasers, optical detection, and bioimaging [1–8]. Among them, bioimaging has attracted much attention for the potential applications in good photostability and co-localization properties in optical imaging analysis instruments, electrophysiology-related surgical devices, and next-generation imaging devices in our daily life. Typical materials developed in this field include organic dyes [9,10], rare-earth compounds [11,12], and semiconductor quantum dots (SQDs) [13–15]. However, the single wavelength, low quantum yield, and complicated/expensive synthesis process limit these materials' wide application and development.

Carbon dots (CDs), widely used in bioimaging, anti-counterfeiting, optoelectronic devices, and other fields because of their rich precursor sources, easy surface functionalization, and excellent physical and chemical properties, is a novel kind of zero-dimensional carbon nano-materials with luminescent properties [16–20]. In these applications, the synthesis of multi-color fluorescent CDs plays a decisive role in multi-channel luminescence and multi-color imaging. Several CDs with bright emissions have been reported to be applied in various fields [20–22]. For example, Lu *et al.* synthesized seven CDs with different fluorescence by adjusting reaction temperature and pH using *o*-phenylenediamine and citric acid as raw materials [20]. Lin *et al.* prepared three types of CDs that had different fluorescence emissions by changing the carbon source (*o*, *m*, and *p*-phenylenediamine) [21]. Tan *et*

* Corresponding authors.
E-mail addresses: xuquan@cup.edu.cn (Q. Xu), luodixian_2@163.com (D. Luo), cailulu@med.uestc.edu.cn (L. Cai).
[1] These authors contributed equally to this work.

https://doi.org/10.1016/j.cclet.2023.108239
1001-8417/

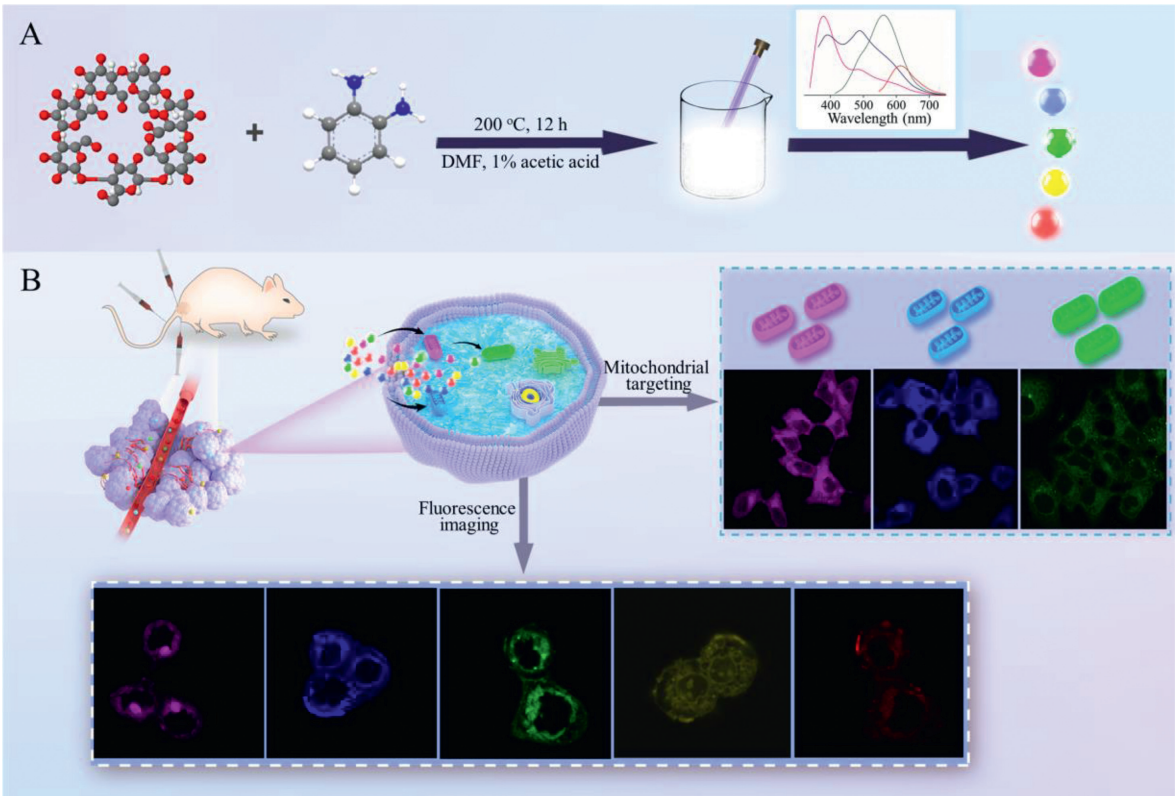

Scheme 1. Synthesis and application of full-spectrum fluorescent CDs. (A) Synthesis route of full-spectrum fluorescent CDs. (B) Application of full-spectrum fluorescent CDs for *in vitro* and *in vivo* imaging.

al. prepared rich color evolution with blue, cyan, green, yellow, and orange by adjusting the pH of the mixed solution of CDs and Rhodamine B [22]. Although these studies have obtained bright photoluminescence multi-color fluorescent CDs, they require a multi-step preparation process and different reaction conditions.

As far as we know, the synthesis methods of multi-color fluorescent CDs need complex reaction conditions and the interference of a variety of external factors as mentioned earlier, which limit the practical development and emission mechanism research of multi-color fluorescent CDs [21–24]. Until now, no experimental work has reported the synthesis of full-spectrum photoluminescent CDs from purple to red fluorescence by a one-step method. Therefore, it is necessary to develop a simple one-step synthesis method to prepare full-spectrum fluorescent CDs to analyze the full-spectrum emission mechanism and its application in suborganelle localization and imaging track.

Herein, we developed a simple method for synthesizing full-spectrum fluorescent CDs using *o*-phenylenediamine, β-cyclodextrin, and *N*,*N*-dimethylformamide (DMF) as raw materials. Under the optimal conditions, the fluorescence quantum yields of the emission peaks at 380, 430, 480, 560 and 613 nm of the full-spectrum fluorescent CDs in DMF solutions were 8.97%, 8.35%, 7.90%, 9.69% and 17.4%, respectively. Due to the high quantum yield and color tunability of full-spectrum fluorescent CDs, the CDs produced bright and steady purple, blue, green, yellow, and red fluorescence in MCF-7 cells, which could realize mitochondria-targeted live-cell imaging and the high-contrast imaging in 4T1 tumor-bearing mice. In summary, the advantages of this work are mainly focus on the synthesis of full-spectrum fluorescent CDs with controllable emission changes from purple (380 nm) and red (613 nm) by a simple and effective method. In addition, in terms of characteristic of full-spectrum fluorescent CDs, the synthesized materials in our work present more fluorescent colors and possess better physicochemical properties, which will further deepen researchers' understanding of the synthesis and application of full-spectrum fluorescent CDs.

Scheme 1 shows the preparation and application of full-spectrum fluorescent CDs. Acetic acid was used as the pH regulator of the solution. *N*,*N*-dimethylformamide was selected as a carbon doping solvent. As carbon sources, *o*-phenylenediamine and β-cyclodextrin could also provide amino/hydroxyl functional groups, which in turn endows full-spectrum fluorescent CDs with better photostability and biocompatibility [25,26]. Interestingly, we found that the content of C=O/C=N/pyrrole N increased first and then reduced with the increase of β-cyclodextrin content (Table S1 in Supporting information), resulting in the fluorescence intensity at the same excitation wavelength at 613 nm first increasing, and then decreasing slightly (Fig. S1 in Supporting information). These results show that N acted on carbon core and functional groups [27,28]. In the carbon core, the pyridine N and pyrrole N defects of N in the carbon core lead to increased fluorescence intensity of the full-spectrum fluorescence CDs at 613 nm. N also existed in the surrounding functional groups in the form of C=N and amide (Table S1), which enhanced the conjugation between C=O and sp^2 carbon core (Fig. S2 in Supporting information) [29]. Moreover, β-cyclodextrin was wrapped on the surface of full-spectrum fluorescent CDs to form a core-shell structure, which was believed that it can effectively reduce flaws and restrain the vibration of the surface groups of the full-spectrum fluorescent CDs, thereupon reducing unrelated non-radiative energy loss [30]. These effects of β-cyclodextrin were well confirmed by comparing fluorescence quantum yields at different ratios (Table S2 in Supporting information). Furthermore, the full-spectrum fluorescent CDs emitted bright and steady purple, blue, green, yellow, and red fluorescence in MCF-7

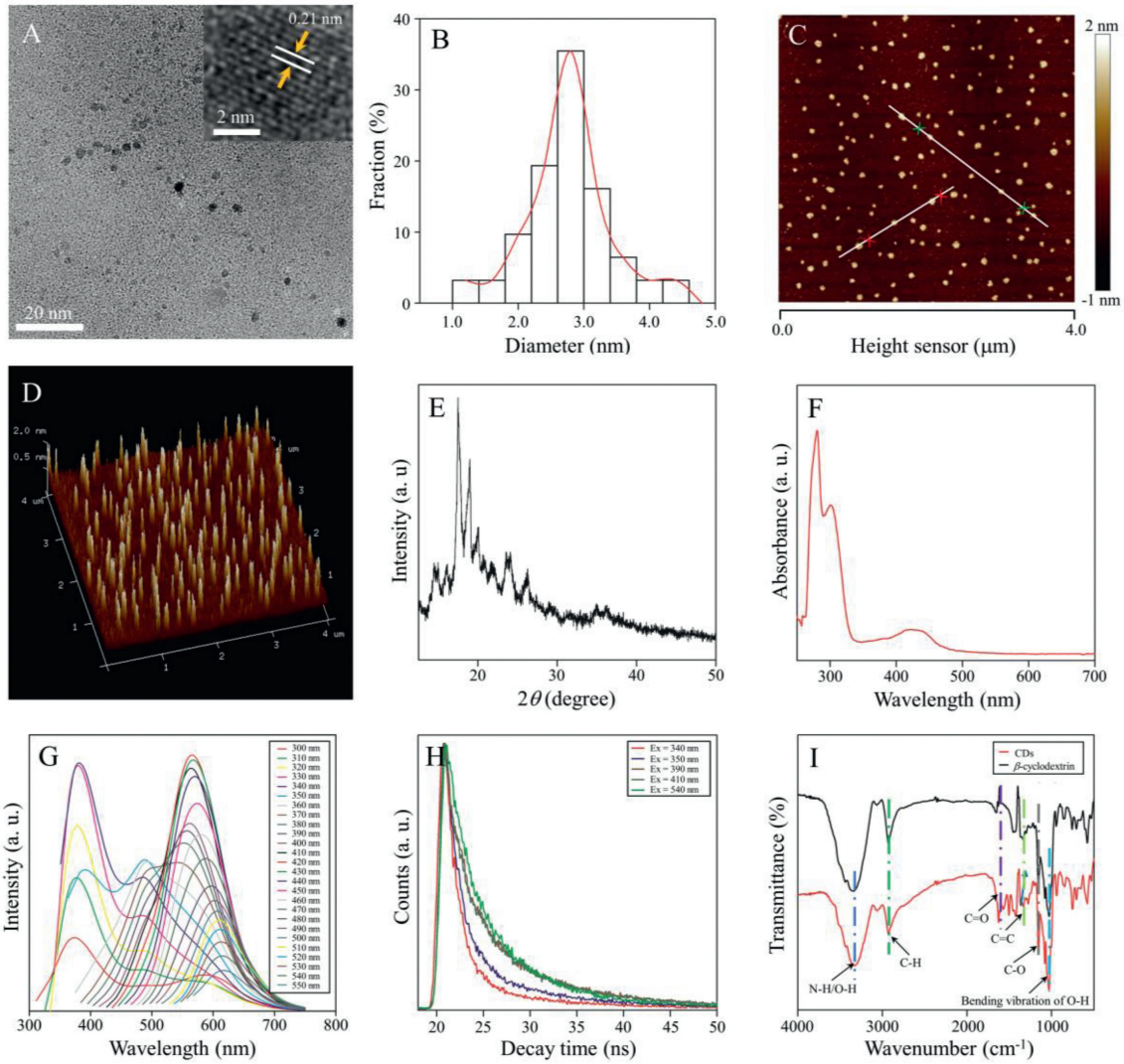

Fig. 1. Morphological and optical properties of full-spectrum fluorescent CDs. (A) HRTEM image. (B) Particle size distribution based on HRTEM detection. (C) AFM image. (D) AFM 3D image. (E) XRD pattern. (F) UV–vis absorption spectra. (G) Fluorescence emission spectra. (H) Time-resolved fluorescence decay curves at different excitation wavelengths. (I) FT-IR spectra of full-spectrum fluorescent CDs and β-cyclodextrin.

cells under optimal conditions, as well as successfully applied for organelle targeting and bioimaging (Scheme 1B).

The structure, morphology, and optical properties of full-spectrum fluorescent CDs prepared from 1.2 g β-cyclodextrin were studied. The TEM image of CDs is shown in Fig. 1A, exhibiting quasi-spherical shapes and even particle size distribution, with an average particle size of 2.6 nm (Fig. 1B). The HRTEM image showed a unique lattice structure with a crystal spacing of 0.21 nm, which was attributed to the (002) crystal plane in graphene [30–32]. As shown in Figs. 1C and D, Figs. S3 and S4 (Supporting information), AFM images further demonstrated that the full-spectrum fluorescent CDs had favorable mono-dispersity and spherical appearance with an average height of 1.8 nm. As shown in Fig. 1E, the XRD pattern of full-spectrum fluorescent CDs presented the strongest peak near 17.5°, indicating good crystallinity, which was a typical feature of CDs [28]. In addition, the UV–vis absorption and fluorescence spectra of full-spectrum fluorescent CDs were investigated at room temperature to assess the optical properties. As displayed in Fig. 1F, the full-spectrum fluorescent CDs solution showed three UV–vis absorption peaks at 279.4, 301.2 and 423.3 nm, which were put down to the n-π^* transition of N or O-based groups, showing that the full-spectrum fluorescent CDs have different electron absorption states [33]. The fluorescence spectra of full-spectrum fluorescent CDs (Fig. 1G) displayed that CDs had multi-color fluorescence emission peaks ranging from 380 nm to 613 nm under different excitation conditions. In addition, Table S3 (Supporting information) in the supporting information shows the detailed fluorescence parameters of the full-spectrum fluorescent CDs. $\Delta\lambda$ ($\Delta\lambda = \lambda_{em} - \lambda_{ex}$, similar to the Stokes shift) increased first and then decreased with the increase of excitation wavelength. The full width at half maximum (FWHM) of the emission spectrum was similar to $\Delta\lambda$ excitation wavelength changes, and the spectral shapes had the property of symmetry. These results indicated that there were multiple emissive domains in CDs, and existed energy transfer among these emission domains [34,35].

The time-resolved fluorescence decay curves of full-spectrum fluorescent CDs were measured at 340, 350, 390, 410 and 540 nm excitation wavelengths, which revealed the deactivation kinetics of electrons from the excited state to the ground state through the radiative and non-radiative pathways. As displayed in Fig. 1H, the fluorescence lifetimes of full-spectrum fluorescent CDs at different excitation wavelengths were 4.77, 6.02, 7.40, 7.42 and 5.94 ns, respectively. Table S4 (Supporting information) summarized the lifetimes, overall contribution, and perfect fit parameters of full-

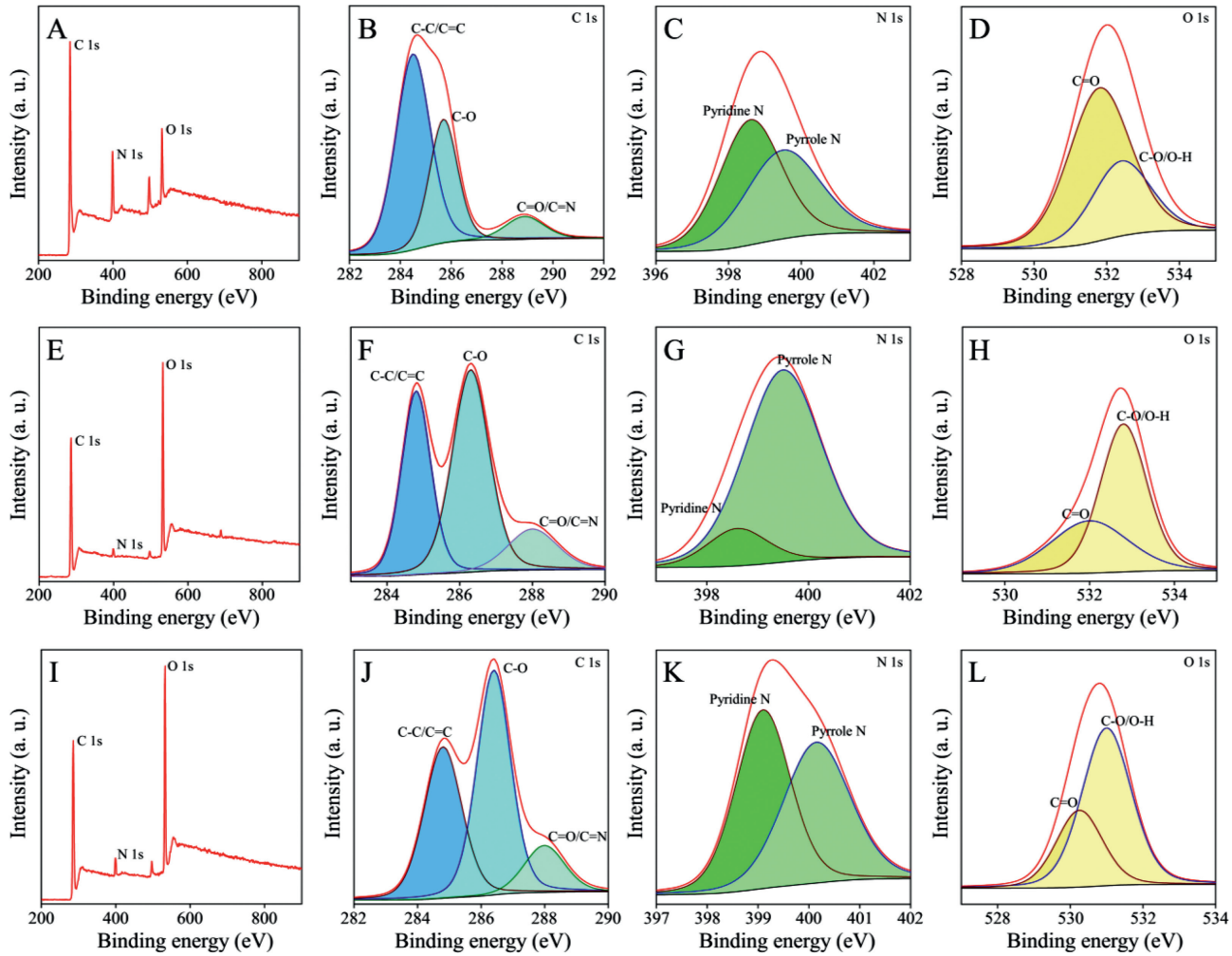

Fig. 2. XPS scan spectra of different prepared CDs. XPS spectra and high-resolution XPS C 1s, N 1s, and O 1s spectra of CDs-1 (A-D), full-spectrum fluorescent CDs (E-H), and CDs-2 (I-L).

spectrum fluorescent CDs at different excitation wavelengths. The results show that with the increase of excitation wavelength, the average lifetime of full-spectrum fluorescent CDs changes from 4.77 ns to 5.94 ns, and the percentage of τ_2 changes from 40.01% to 61.37%, indicating that the carbon core of the full-spectrum fluorescent CDs plays an important role in the radiation lifetime at 410 nm [36,37]. These findings demonstrated that the prepared full-spectrum fluorescence CDs possessed excellent optical properties with the tunable fluorescence emission related to carbon cores. Figs. S5-S7 (Supporting information) show the photostability of full-spectrum fluorescent CDs at different pH values, times, and salt solution concentrations under different excitation wavelengths. In Fig. S5, the fluorescence intensity of full-spectrum fluorescent CDs at 340, 350 and 540 nm excitation wavelength remains unchanged with the increase of pH value. In contrast, the fluorescence intensity of full-spectrum fluorescent CDs at 390 and 410 nm excitation wavelength was decreased to 61.3% and 48.5% of the original fluorescence intensity, respectively. At the same time, under light conditions, the full-spectrum fluorescent CDs under different excitation wavelengths remained almost unchanged during continuous fluorescence spectra tests with different times and salt solution concentrations (Figs. S6 and S7), indicating that the full-spectrum fluorescent CDs had high optical stability. Moreover, the quantum yields of full-spectrum fluorescent CDs at 340, 350, 390, 410 and 540 nm were measured by a spectrometer equipped with an integrating sphere, and the corresponding quantum yields were 8.97%, 8.35%, 7.90%, 9.69% and 17.4%, respectively. Due to their high quantum yield, multi-color fluorescence, and simple preparation method, full-spectrum fluorescent CDs and their modified nanomaterials showed the potential for being used in organelle targeting and biological imaging [22,38,39].

β-Cyclodextrin, a special molecular structure consisting of the hydrophobic lumen and hydrophilic outer surface, has been used in biosensing and drug delivery through competitive host-client interactions with dye molecules and therapeutic agents [40,41]. In this study, β-cyclodextrin and *o*-phenylenediamine were used as precursors to prepare the full-spectrum fluorescent CDs. Hydrothermal treatment of each precursor alone resulted in lower quantum yield and less color fluorescence of our CDs (CDs-1 and CDs-3) compared with the combination of the two precursors (Figs. S1A and S8 in Supporting information), which might be due to the β-cyclodextrin linking multiple *o*-phenylenediamine molecules *via* hydroxyl groups. FT-IR and XPS were further applied to study the factors affecting the luminescence of full-spectrum fluorescent CDs (Figs. 1I and 2, Fig. S9 in Supporting information). According to the frequency fluctuations of 3365 cm^{-1}, 2924 cm^{-1}, 1642 cm^{-1}, 1500 cm^{-1}, and 1138 cm^{-1} observed by FT-IR, we can conclude that they were attributed to N–H/O–H, C–H, C=O, C=C, and C–O, respectively [41–43]. However, the strong vibration peaks of the β-cyclodextrin and full-spectrum fluorescent CDs at 1045 cm^{-1} were

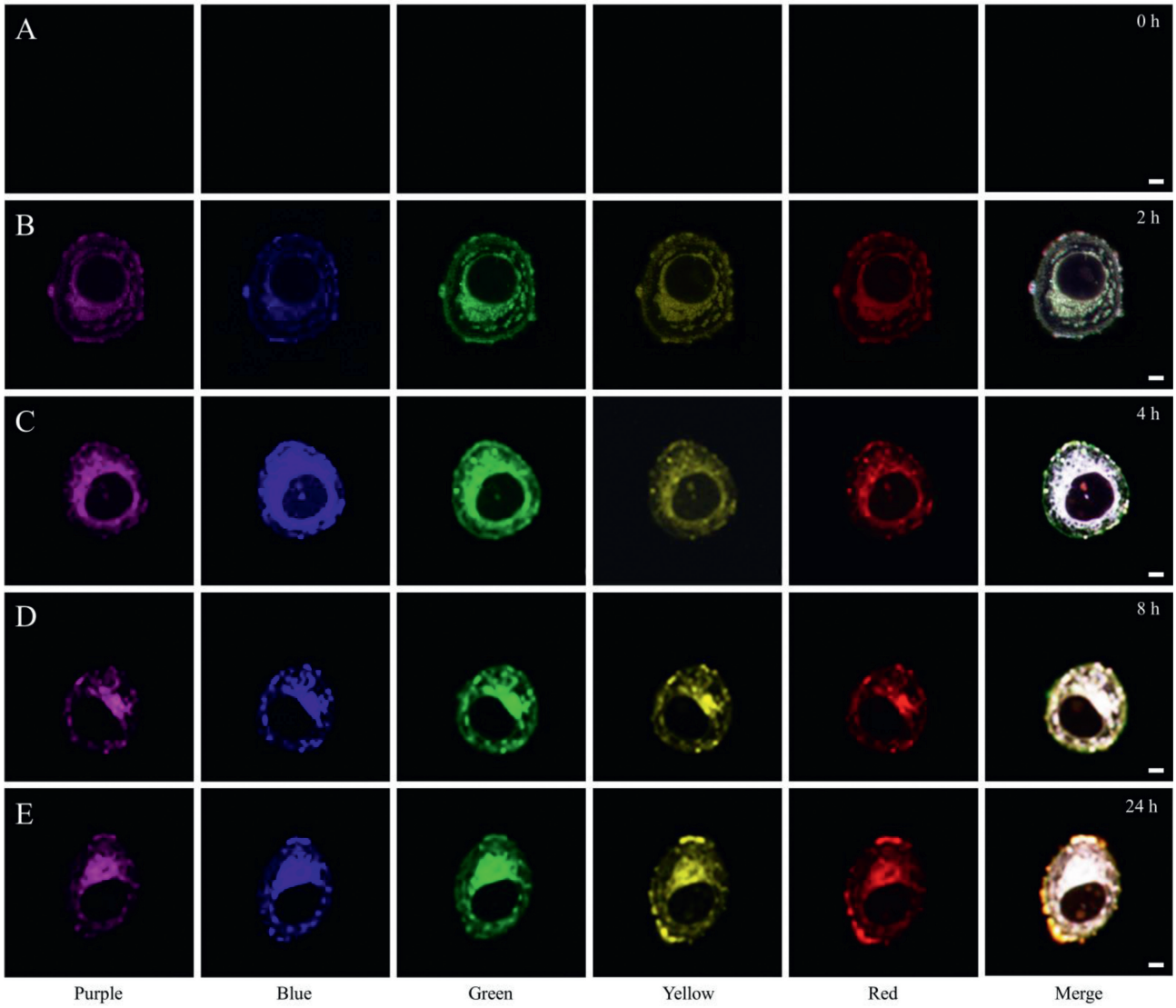

Fig. 3. Fluorescence images of MCF-7 cells incubated with full-spectrum fluorescent CDs at 0 (A), 2 (B), 4 (C), 8 (D), and 24 h (E). Scale bar: 5 μm.

attributed to the bending vibration of O–H, and the vibration peaks of CDs-1 and CDs-2 at 3147 cm^{-1} were due to stretching vibration of =C–H. The intensities of the C=C vibrational peaks in CDs-1 and CDs-2 spectra were more significant than that of the corresponding peaks in β-cyclodextrin and full-spectrum fluorescent CDs spectra, but for β-cyclodextrin and full-spectrum fluorescent CDs, the absorption band of N–H/O–H became wider, indicating that the large N–H/O–H groups on the surface of full-spectrum fluorescent CDs [44]. The XPS full scan spectra (Figs. 2A, E and I) demonstrated that the three kinds of CDs mainly consisted of C, N and O, and the atomic concentrations of different elements were displayed in Table S5 (Supporting information). As shown in Figs. 2B, F and J, the high-resolution XPS C 1s spectra showed three binding energies, 284.7, 286.3 and 288.2 eV, corresponding to the vibrations of C–C/C=C, C–O, and C=O/C=N, respectively [14]. Among them, the proportion of C–C/C=C decreased from 56.8% to 35.4% and 36.8%, and the ratio of C=O/C=N increased from 11.7% to 14.4% and 13.1%, respectively, as shown in Table S1. The high-resolution XPS N 1s spectra could be divided into two components, 398.6 and 399.5 eV, which were associated with the pyridine N and pyrrole N bands, respectively (Figs. 2C, G and K). The high-resolution XPS O 1s spectra (Figs. 2D, H and L) presented two peaks at 532.2 and 532.9 eV corresponding to the C=O and C–O/O–H bands, respectively [45,46]. Overall, these functional groups detected from XPS spectra were consistent with those observed in FT-IR spectra, indicating that the full-spectrum fluorescent CDs possessed a broad range of conjugated sp^2 domains, including many O- and N-containing surface groups.

The optical properties and structural characterization of full-spectrum fluorescent CDs (Figs. 1G and 2, Figs. S5-S7) indicated that the prepared CDs endowed beneficial solubility, photostability, and special full-spectrum properties, which emerged with enormous potential in biological applications [33,47,48]. MCF-7 cells were used to evaluate the cytotoxicity of CDs through the standard MTT assay (Fig. S10 in Supporting information). The cells were co-cultured with different concentrations of full-spectrum fluorescent CDs (0.0, 0.0625, 0.125, 0.25, 0.5, 0.75, 1.0, 1.25, 1.5, 1.75 and 2.0 mg/mL, respectively) for 24 h. The results showed that MCF-7 cells still had more than 90% cell survival rate even at the CD concentration of 0.5 mg/mL, indicating reliable cytocompatibility and low biotoxicity.

We further evaluated the imaging ability of full-spectrum fluorescent CDs in MCF-7 cells by confocal laser scanning microscopy (CLSM). MCF-7 cells were cultured for 24 h, followed by treat-

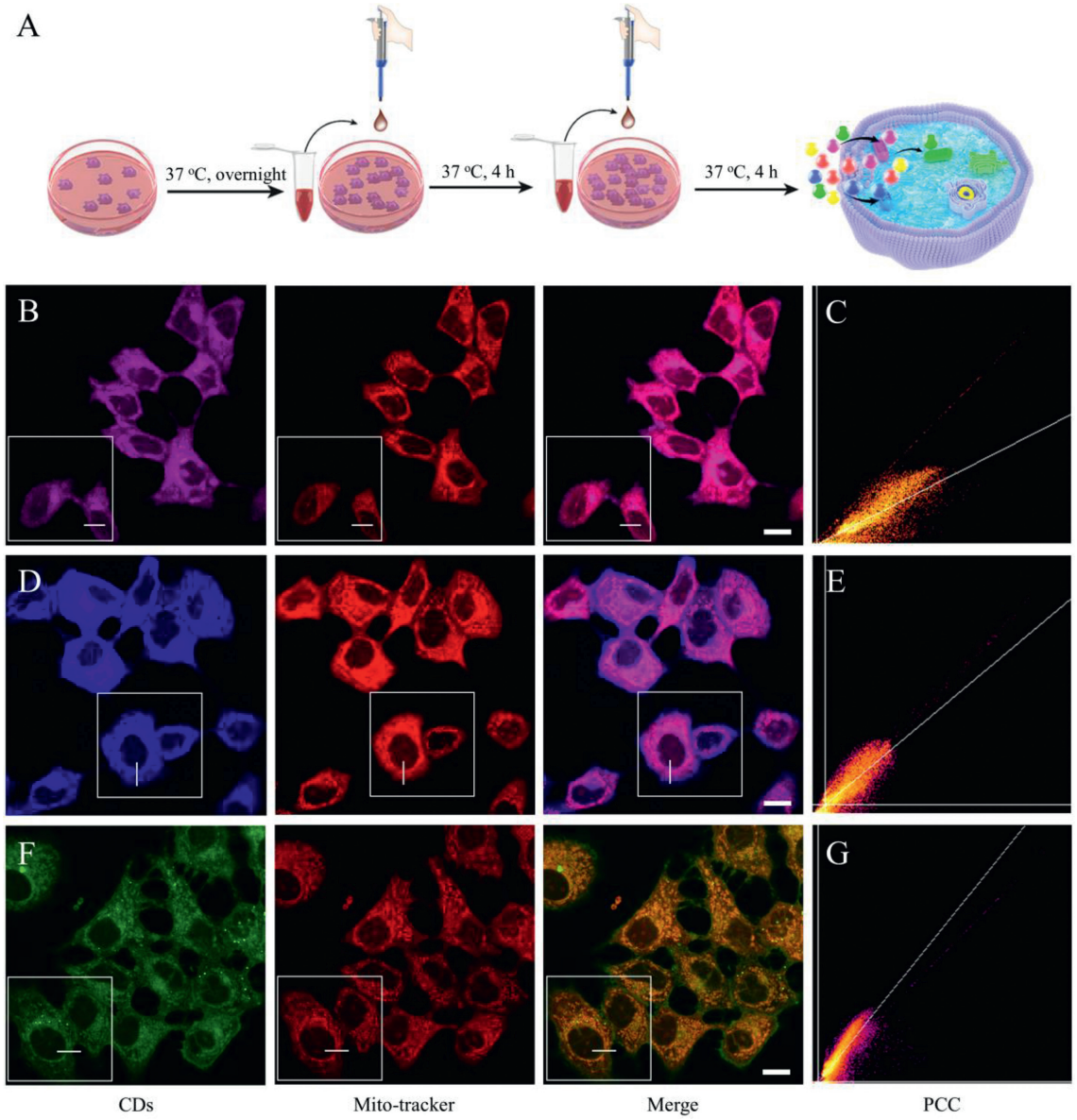

Fig. 4. Full-spectrum fluorescent CDs were used for fluorescence imaging of mitochondria. (A) Schematic diagram of mitochondrial imaging using full-spectrum fluorescent CDs. (B, C) Confocal fluorescence images and Pearson's correlation coefficient diagram of MCF-7 cells stained with purple fluorescent CDs and Mito-Tracker. (D, E) Confocal fluorescence images and Pearson's correlation coefficient diagram of MCF-7 cells stained with blue fluorescent CDs and Mito-Tracker. (F, G) Confocal fluorescence images and Pearson's correlation coefficient diagram of MCF-7 cells stained with green fluorescent CDs and Mito-Tracker. Scale bar: 10 μm.

ment with full-spectrum fluorescent CDs at various concentrations (0.0, 0.125, 0.25 and 0.5 mg/mL) for 4 h. As the concentration of full-spectrum fluorescent CDs increased from 0.0 to 0.5 mg/mL, the fluorescence intensity in MCF-7 cells gradually increased (Fig. S11 in Supporting information). Moreover, the mitochondria and cell membranes of the MCF-7 cells could also be observed with multiple colors under different excitation wavelengths (Fig. S12 in Supporting information). To further explore the factors leading to the above results, the zeta potential and FT-IR spectrum of full-spectrum fluorescent CDs were measured, and the results were displayed in Fig. S13 (Supporting information) and Fig. 1I. The zeta potential of full-spectrum fluorescent CDs was 1.2 mV, which could be explained by the fact that *o*-phenylenediamine, a carboxy-free raw material, contains a large number of amino functional groups. Moreover, the corresponding FT-IR spectrum in the 1600–1400 cm^{-1} region confirmed that the CDs had a benzene ring. Therefore, the full-spectrum fluorescent CDs with positive charge were adsorbed on the surface of the cell membrane through electrostatic interaction and facilitated cellular uptake [49]. Subsequently, we investigated the uptake efficiency of full-spectrum fluorescent CDs by MCF-7 cells at different periods (2, 4, 8, and 24 h). As shown in Fig. 3 and Fig. S14 (Supporting information), with the incubation time increases, the fluorescence colors of purple, blue, green, yellow, and red were slightly weakened, and the corresponding fluorescence intensity was slightly decreased (Fig. S15 in Supporting information), which further indicated that the full-spectrum fluorescent CDs had better photostability [50,51].

To further explore the targeting ability of full-spectrum fluorescent CDs to the mitochondria. MCF-7 cells were co-incubated with full-spectrum fluorescent CDs for 4 h, and then stained with mitochondria-specific dye (Mito-Tracker) (Fig. 4A). To avoid the effect of spectral overlap between CDs and Mito-Tracker, we optimized the respective imaging conditions so that CLSM could only perform fluorescence emission from the desired dye imaging, re-

ducing experimental errors. From the CLSM images, we found the purple, blue and green fluorescence emitted by CDs could mostly overlap with the red fluorescence emitted by Mito-Tracker (Figs. 4B, D and F). Furthermore, Pearson's correlation coefficient (PCC) was also calculated according to the correlation diagram between full-spectrum fluorescent CDs and Mito-Tracker for analysis (Figs. 4C, E and G). It was found that the PCC values of the full-spectrum fluorescent CDs-Mito-Tracker group were 0.892, 0.903 and 0.92, respectively. They indicated that the full-spectrum fluorescent CDs almost only stained the mitochondria. In addition, to better evaluate the subcellular localization of full-spectrum fluorescent CDs, we also performed quantitative fluorescence analysis on cell-specific sites in CDs, Mito-Tracker, and Merge group. As shown in Figs. S16 and S17 (Supporting information), the purple, blue, and green fluorescence signals from the full-spectrum fluorescence CDs and red fluorescence signals from the Mito-Trackers within the mitochondria of dormant MCF-7 cells were well overlapped. Moreover, the fluorescence intensity of mitochondria in the Merge group was much higher than that in the CDs and Mito-Tracker groups (Fig. S17), indicating a synergistic enhancement mechanism between the full-spectrum fluorescent CDs and Mito-Tracker. The selective targeting ability of full-spectrum fluorescent CDs to mitochondria could be explained by the full delocalization, lipophilicity, and positive charge properties of CDs, which have been reported as prerequisites for good ligand interactions with mitochondria [49,52,53].

Long-wavelength emitting dyes can minimize the interfering effects of phototoxicity of biological samples and tissue background autofluorescence [14,54,55]. Encouraged by the success of *in vitro* cell imaging based on full-spectrum fluorescent CDs, we further explored whether full-spectrum fluorescent CDs were eligible for targeted imaging *in vivo*. We examined the imaging effects of full-spectrum fluorescent CDs after subcutaneous, intratumoral, and intravenous injection to 6-week-old female 4T1 tumor-bearing Balb/C mice. Animal experiments were conducted following the guidelines for the use and care of animals issued by the Animal Ethics Committee of Huazhong University of Science and Technology Union Shenzhen Hospital. The mice tumor areas injected through the subcutaneous (Fig. S18A in Supporting information) and the tumor (Fig. S18B in Supporting information) emitted bright red fluorescence. Over time, the fluorescent intensity gradually decreased, as seen in the tumor area. Therefore, the fluorescence signal of full-spectrum fluorescent CDs has favorable signal-to-noise at excitation and emission wavelengths of 540 and 600 nm, indicating that the full-spectrum fluorescent CDs had good potential applicability for *in vivo* imaging. However, the tumor areas of the mice injected with the caudal vein didn't emit bright red fluorescence but emitted red fluorescence on the back and forelimbs of the mice (Fig. S19 in Supporting information). Therefore, further optimizing the reaction conditions and raw material formulation is necessary to prepare specific targeted full-spectrum fluorescent CDs, accelerating the pace of fluorescence imaging tracking *in vivo*.

In conclusion, we successfully synthesized a type of full-spectrum fluorescent CDs with controlled emission color changes from purple to red by self-doping with *o*-phenylenediamine, β-cyclodextrin, and *N*,*N*-dimethylformamide as raw materials. Combined with the experimental results, we found that the excitation dependence of CDs was closely related to regulating sp^3 and sp^2 hybrid carbons in the β-cyclodextrin-related groups on their surfaces. Moreover, the optimal quantum yields of CDs at excitation wavelengths of 340, 350, 390, 410 and 540 nm were 8.97%, 8.35%, 7.90%, 9.69% and 17.4%, respectively. With regard to the high quantum yield and color tunability, the CDs were successfully used for mitochondrial co-localization imaging with different fluorescence colors and high-contrast imaging of 4T1 tumor-bearing mice with different injection forms. However, the limitation that the tumor areas of mice injected into the caudal vein could not emit bright red fluorescence was due to the problem of specific targeting of CDs. Our findings not only provide a new idea for multi-color fluorescent carbon nanomaterials but also deepen the application potential of carbon nanomaterials by researchers.

Declaration of competing interest

The authors declare that they have no known competing financial interests or personal relationships that could have appeared to influence the work reported in this paper.

Acknowledgments

This research was supported by the National Natural Science Foundation of China (No. U2230123), the Science Foundation of the Science and Technology Department of Sichuan Province (No. 22ZYZYTS0159), Science Foundation of China University of Petroleum (Nos. 2462019QNXZ02, 2462019BJRC007), Science Foundation of China University of Petroleum (East China) (No. 2462020YXZZ018), Science and Technology Innovation Commission of Shenzhen (No. JSGG20210802153410031), Science and Technology Project of Nanshan District (No. NS2021016), and the Scientific Research Startup Fund for Discipline Leader of Huazhong University of Science and Technology Union Shenzhen Hospital (Nanshan Hospital) (No. YN2021002).

Supplementary materials

Supplementary material associated with this article can be found, in the online version, at doi:10.1016/j.cclet.2023.108239.

References

[1] K. Kim, P. Dannenberg, H. Yan, et al., Adv. Funct. Mater. 31 (2021) 2103413.
[2] K. Keevend, L. Puust, K. Kurvits, et al., Nano Lett. 19 (2019) 6013–6018.
[3] X. He, S. Wu, Q. Liao, et al., J. Mater. Chem. C 5 (2017) 12707–12713.
[4] E. Soheyli, S. Behrouzi, Z. Sharifirad, et al., Ceram. Int. 45 (2019) 11501–11507.
[5] H. Zhang, G. Li, Y. Zhu, et al., Chem. Eng. J. 380 (2020) 122491.
[6] E. Song, Y. Wang, W. Hu, et al., Biosens. Bioelectron. 72 (2015) 320–325.
[7] Y.C. Niu, J.J. Gao, L.L. Cai, et al., Nano Res. 14 (2021) 3820–3839.
[8] X. Yang, X. Li, S. Lu, et al., Chin. Chem. Lett. 33 (2022) 613–625.
[9] H. Cheng, B. Tang, J. Yoon, et al., Chem. Soc. Rev. 49 (2020) 21–31.
[10] Z. Lei, P. Pei, S. Wang, et al., Angew. Chem. Int. Ed. 58 (2019) 8166–8171.
[11] C. Ding, C. Zhang, T. He, et al., Nanoscale 9 (2017) 14031–14038.
[12] Y.N. Chouryal, R.K. Sharma, H.L. Kewat, et al., Biomater. Sci. 8 (2020) 6730–6740.
[13] J. Wang, Y. Lu, F. Peng, et al., Biomaterials 34 (2013) 9509–9518.
[14] W. Gao, X. Wang, X. Liu, et al., ACS Appl. Mater. Interfaces 10 (2018) 1147–1154.
[15] X. Yan, J.F. Ma, L.L. Cai, et al., Chin. Chem. Lett. 31 (2020) 3173–3177.
[16] P.D. Zhu, X.L. Zhao, M. Xu, et al., Front. Bioeng. Biotechnol. 10 (2022) 964814.
[17] J. Chen, N. Yuan, H. Qiu, et al., Chin. Chem. Lett. 32 (2021) 3398–3401.
[18] X. Geng, Y.F. Guo, Y. Wang, et al., Adv. Funct. Mater. 32 (2022) 2206753.
[19] Z. Wang, X. Li, Y. Li, et al., Adv. Mater. 29 (2017) 1702910.
[20] M.R. Zhang, R.G. Su, Q. Xu, et al., Nano Res. 12 (2019) 815–821.
[21] K. Jiang, L. Zhang, Y. Lu, et al., Angew. Chem. Int. Ed. 54 (2015) 5360–5363.
[22] P. Zhu, L. Gao, J. Xiong, et al., ACS Appl. Mater. Interfaces 13 (2021) 33354–33362.
[23] B.Y. Wang, S.Y. Lu, Matter 5 (2022) 110–149.
[24] H. Nie, M. Li, S. Liang, et al., Chem. Mater. 26 (2014) 3104–3112.
[25] B. Wang, Z. Wei, L. Sui, et al., Light Sci. Appl. 11 (2022) 14.
[26] X. Wu, Y. Wang, J. Zhu, et al., Biosens. Bioelectron. 90 (2016) 501–507.
[27] M. Sudolská, M. Otyepka, Appl. Mater. Today 7 (2017) 190–200.
[28] Z.H. Sheng, L. Shao, J.J. Chen, et al., ACS Nano 5 (2011) 4350–4358.
[29] L. Li, B. Yu, T. You, et al., Biosens. Bioelectron. 74 (2015) 263–269.
[30] Y. Zhang, L. Wang, J. Yu, et al., Angew. Chem. Int. Ed. 60 (2021) 25514–25521.
[31] D. Qu, J. Li, Z. Xie, et al., Light Sci. Appl. 4 (2015) e364.
[32] X. Yang, L. Ai, S. Lu, et al., Sci. Bull. 67 (2022) 1450–1457.
[33] E.S. He, H.J. Wang, Q.X. Mao, et al., ACS Nano 15 (2021) 14465–14474.
[34] B. Ju, H. Nie, Z. Liu, et al., Nanoscale 9 (2017) 13326–13333.
[35] B. Ju, H. Nie, X.G. Zhang, et al., ACS Appl. Nano Mater. 1 (2018) 6131–6138.
[36] H. Ding, S. Yu, H. Xiong, et al., ACS Nano 10 (2016) 484–491.
[37] F. Ehrat, S. Bhattacharyya, J. Schneider, et al., Nano Lett. 17 (2017) 7710–7716.
[38] B. Zhi, X. Yao, Q. Cui, et al., Chem. Sci. 12 (2021) 2441–2455.
[39] J. Zhan, B.J. Geng, K. Wu, et al., Carbon 130 (2018) 153–163.
[40] M. Luo, Y. Hua, Y. Liang, et al., Biosens. Bioelectron. 98 (2017) 195–201.

[41] U. Baruah, N. Gogoi, G. Majumdar, et al., Carbohydr. Polym. 117 (2015) 377–383.
[42] X. Chen, Q. Jin, L. Wu, et al., Angew. Chem. Int. Ed. 53 (2014) 12542–12547.
[43] J. Zhong, X.M. Chen, M.R. Zhang, et al., Chin. Chem. Lett. 31 (2020) 201–205.
[44] X. Ye, Y. Xiang, Q. Wang, et al., Small 15 (2019) e1901673.
[45] Y. Zhan, T. Geng, Y.L. Liu, et al., ACS Appl. Mater. Interfaces 10 (2018) 27920–27927.
[46] G. Zou, S. Chen, N. Liu, et al., Chin. Chem. Lett. 33 (2022) 778–782.
[47] X. Geng, Y. Sun, Z. Li, et al., Small 15 (2019) e1901517.
[48] Y.Q. Sun, H.Y. Qin, X. Geng, et al., ACS Appl. Mater. Interfaces 12 (2020) 31738–31744.
[49] X.W. Hua, Y.W. Bao, Z. Chen, et al., Nanoscale 9 (2017) 10948–10960.
[50] R. Ye, C. Xiang, Z. Yan, et al., Nat. Commun. 4 (2013) 2943.
[51] Z. Tu, K. Achazi, A. Schulz, et al., Adv. Funct. Mater. 27 (2017) 1701837.
[52] M.J. Weiss, J.R. Wong, C.S. Ha, et al., Proc. Nat. Acad. Sci. U. S. A. 84 (1987) 5444–5448.
[53] V. Weissig, V.P. Torchilin, Adv. Drug Deliv. Rev. 49 (2001) 127–149.
[54] P.L. Gao, J.W. Wang, M. Zheng, et al., Chem. Eng. J. 381 (2020) 122665.
[55] X.W. Hua, Y.W. Bao, J. Zeng, et al., ACS Appl. Mater. Interfaces 11 (2019) 32647–32658.